AD-A055 576 ARMY MATERIALS AND MECHANICS RESEARCH CENTER WATERTO--ETC F/G 11/6
SOLIDIFICATION OF ELECTROSLAG REMELTED LOW ALLOY STEEL INGOTS.(U)
OCT 77 R H FROST

UNCLASSIFIED AMMRC-TR-77-20 NL

| OF |
AD
A055 576

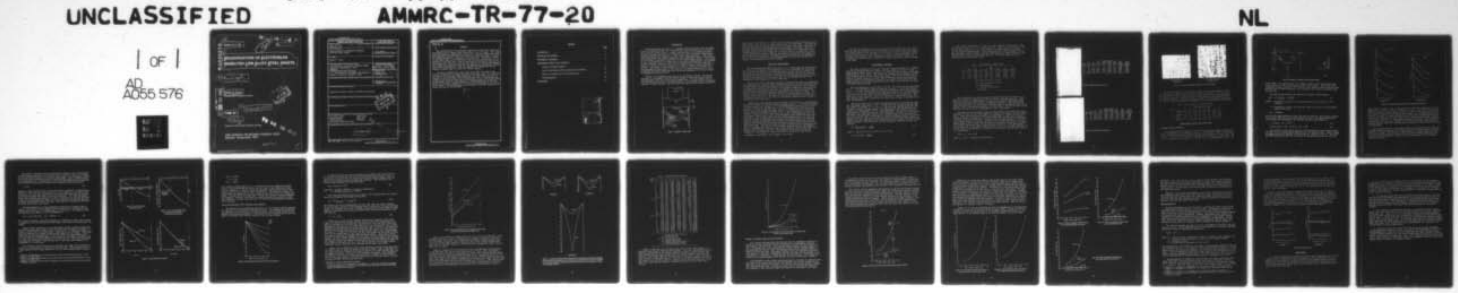

END
DATE
FILMED
8-78
DDC

AMMRC-TR-77-20

SOLIDIFICATION OF ELECTROSLAG REMELTED LOW ALLOY STEEL INGOTS

Final rept.,

ROBERT H. FROST
PROCESS DEVELOPMENT DIVISION

1T162105AH84

October 1977

27 p.

ARMY MATERIALS AND MECHANICS RESEARCH CENTER
Watertown, Massachusetts 02172

UNCLASSIFIED

SECURITY CLASSIFICATION OF THIS PAGE (When Data Entered)

REPORT DOCUMENTATION PAGE		READ INSTRUCTIONS BEFORE COMPLETING FORM
1. REPORT NUMBER AMMRC TR 77-20	2. GOVT ACCESSION NO.	3. RECIPIENT'S CATALOG NUMBER
4. TITLE (and Subtitle) SOLIDIFICATION OF ELECTROSLAG REMELTED LOW ALLOY STEEL INGOTS		5. TYPE OF REPORT & PERIOD COVERED Final Report 6. PERFORMING ORG. REPORT NUMBER
7. AUTHOR(s) Robert H. Frost		8. CONTRACT OR GRANT NUMBER(s)
9. PERFORMING ORGANIZATION NAME AND ADDRESS Army Materials and Mechanics Research Center Watertown, Massachusetts 02172 DRXMR-ER		10. PROGRAM ELEMENT, PROJECT, TASK AREA & WORK UNIT NUMBERS D/A Project: 1T162105AH84 AMCMS Code: 612105.11.H84 Agency Accession: DA OE4812
11. CONTROLLING OFFICE NAME AND ADDRESS U. S. Army Materiel Development and Readiness Command, Alexandria, Virginia 22333		12. REPORT DATE October 1977 13. NUMBER OF PAGES 25
14. MONITORING AGENCY NAME & ADDRESS(if different from Controlling Office)		15. SECURITY CLASS. (of this report) Unclassified 15a. DECLASSIFICATION/DOWNGRADING SCHEDULE

16. DISTRIBUTION STATEMENT (of this Report)

Approved for public release; distribution unlimited.

17. DISTRIBUTION STATEMENT (of the abstract entered in Block 20, if different from Report)

18. SUPPLEMENTARY NOTES

19. KEY WORDS (Continue on reverse side if necessary and identify by block number)

Low alloy steels
Microstructure
Solidification
Electroslag remelting (ESR)
Fluid flow
Heat flow
Refining

20. ABSTRACT (Continue on reverse side if necessary and identify by block number)

(SEE REVERSE SIDE)

DD FORM 1 JAN 73 1473 EDITION OF 1 NOV 65 IS OBSOLETE

UNCLASSIFIED

SECURITY CLASSIFICATION OF THIS PAGE (When Data Entered)

Block No. 20

ABSTRACT

The solidification of electroslag remelted AISI 4340 steel ingots was investigated over a range of melt rates from 3.7 to 6.3 lb/min. The liquid metal pool shape was determined by marking the liquidus isotherm with tungsten additions, and these data were used for an empirical model to predict the liquidus geometry as a function of the melt rate. The model is based on the premise that the solidification rate normal to the mold wall is independent of the melt rate. Data on the local solidification time and the axial mushy zone width were obtained from dendrite arm spacing measurements and an empirical relation between the arm spacings and the average cooling rate during solidification. This was combined with information on the liquidus isotherm shape to locate the solidus isotherm.

The local solidification time, mushy zone width, and depth of the solidus isotherm are not linear functions of the melt rate. At a high melt rate where the liquid pool depth approaches the ingot radius the rate of increase of these variables with increasing melt rate is significant, and conditions are produced which would be expected to result in solidification-related defects such as macrosegregation. Macrosegregation was investigated by wet chemical analyses at locations from the surface to the center of the ingots. No macrosegregation was observed in the AISI 4340 alloy at either the high or low melt rate.

CONTENTS

INTRODUCTION

Electroslag remelting (ESR) is a secondary remelting process used to produce ingots with refined directional structures which are free from porosity and pipe, have excellent surface quality, minimal cropping losses, low sulfide and oxide inclusion contents from chemical refining by the slag, and greatly reduced macrosegregation problems as compared to other ingot casting processes. Ingot structure, cleanliness, and chemical homogeneity have significant effects on the levels and anisotropy of mechanical properties in the final wrought product. The purpose of this investigation is to characterize the solidification geometry and structure, thermal gradients, chemistry, and chemical homogeneity of AISI 4340 steel ESR ingots as a function of the melting rate in order to predict optimum melting conditions. The results of this analysis will serve as the basis for studies of macrosegregation using ingots of the same size; the models generated will allow prediction of process conditions under which macrosegregation is likely to occur in segregation-sensitive alloys.

Figure 1 is a schematic cross section of an ESR melt station. The process consists of a consumable electrode melted through a resistively heated calcium fluoride-based slag into a water-cooled copper mold. The thin molten layer on the immersed portion of the electrode provides a large surface area for slag-metal chemical refining reactions, and the heated slag pool provides thermal inertia to

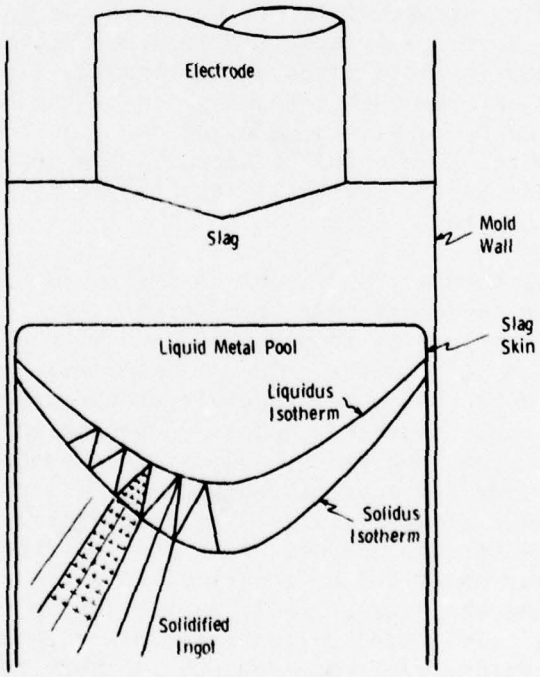

Figure 1. Schematic of ESR process.

dampen process instabilities. A thin slag layer which solidifies between the mold wall and the ingot provides a smooth surface typical of ESR ingots. The shape and depth of the molten metal pool (defined by the liquidus and solidus isotherms) is of prime importance in determining the cast structure of the ingot. The size of the mushy zone between the liquidus and solidus isotherms is a function of the thermal gradients and the melting rate. The time spent in the mushy zone (local solidification time) can be related to the dendrite arm spacing or coarseness of the solidification structure. The geometries and velocities of the isotherms affect the velocity and direction of the interdendritic fluid flow and hence the extent of macrosegregation of alloy elements.

OBJECTIVES AND APPROACH

The investigation had three objectives: (1) to investigate the liquid metal pool profile as a function of the melting rate; (2) to determine the solidification structure and geometry including the location of the solidus isotherm, the shape and velocity of the mushy zone between the liquidus and solidus isotherms, and the local solidification time as functions of the melting rate and the solidification characteristics of the alloy; and (3) to investigate the melt-rate dependence of macrosegregation in AISI 4340 steel.

The velocity of the slag/metal interface and the melting rate were determined experimentally from readings of the electrode position at one minute intervals and a volume balance based on measurements of the electrode and ingot cross sections. The liquid metal pool profile (given by the liquidus isotherm) was determined experimentally at high and low melt rates by marking the liquidus isotherm with tungsten additions and metallographic examination of the sectioned ingots. This data was used to develop an empirical model of the liquid metal pool shape as a function of the melt rate. The model is based on the observation that the rate of solidification normal to the mold wall (transverse solidification velocity) is independent of the melt rate.

Information on the thermal conditions during solidification is experimentally difficult to obtain for the electroslag remelting process. A traditional approach for teemed ingots and castings is to use imbedded thermocouples to provide information in the form of cooling curves. This is hampered for the ESR process by problems of access through the copper crucible or through the slag layer which rapidly erodes thermocouple protector tubes. A second approach is to mark the liquidus isotherm by various additions, and use this experimental data for the correction of quasi-steady state or time-dependent finite difference heat transport models. The present study utilizes a third approach which is to mark the liquidus isotherm by additions, and calculate the solidification rate from dendrite arm spacing measurements and an empirical relation between the secondary dendrite arm spacing and the average cooling rate during solidification for the particular alloy. The calculated cooling rates are then used in combination with data on the shape and velocity of the liquidus isotherm from the experimental marks to determine the location of the solidus isotherm, width of the mushy zone, and the local solidification time. This approach was used by Mellberg and Sandberg[1] to investigate the solidification of M-2 high-speed steel ingots.

1. MELLBERG, P. O., and SANDBERG, H. Scand. J. Metallurgy, v. 2, 1973, p. 83-86.

The melt-rate dependence of macrosegregation in AISI 4340 steel was investigated by chemical analysis of the ingots melted at the highest and lowest rates. Wet chemical analyses were performed on drilled chips taken at increments along a line from the surface to the center of the ingot, at an ingot height of 25 cm from the starting plate. Macrosegregation caused by the flow of solute-rich interdendritic liquid would be evidenced by chemical variations across the width of the ingot.

EXPERIMENTAL PROCEDURE

The study is based on 300-lb AISI 4340 steel ingots produced with a CONSARC electroslag remelting furnace at AMMRC. The ingots had an 8 inch by 8 inch round-cornered square cross section with an area of 58 square inches, and heights ranging from 18 to 20 inches. The furnace was equipped for independent continuously variable control of the current and voltage. The current control was provided by saturable reactors in series with the primary side of the transformer. Voltage control was provided by a feedback loop coupled to the hydrolytic electrode suspension system which positions the electrode in the slag pool to match a desired reference voltage.

The slag composition was 70% CaF_2 + 15% CaO + 15% Al_2O_3, and the slag charge was 18 lb which provided a slag pool depth of 3 inches. A cold slag start-up procedure was used, and the melts were terminated abruptly with no hot-topping. A high power level was required during start-up because of the chilling effect of the mold bottom and the heat of fusion required to melt the slag charge. After start-up the power input was controlled to maintain a constant melt rate, and power changes were made by adjusting both current and voltage to maintain a constant melt geometry.

Records were kept of the weights and dimensions of the electrode and ingot, the slag charge, the weights of the starting plate and the final slag cap, and the maximum slag height in the crucible. The melt log recorded during the melt included: current, voltage, power, electrode position, the entrance and exit cooling water temperatures, and the slag temperature. The melting rate M in pounds per minute and the velocity of the slag/metal interface V_I in centimeters per minute were calculated from the cross-sectional area of the electrode A_e, the cross-sectional area of the ingot A_i, and the electrode velocity V_E in centimeters per minute. The electrode velocity was determined from least-squares regression fits of electrode position measurements to the nearest 0.01 inch at one-minute intervals. The melting rate and the slag/metal interface velocity are given by:

$$M = [(A_e A_i \rho)/(A_i - A_e)]V_E \qquad (1)$$

where ρ = density of steel (0.283 lb/cu in.), and

$$V_I = [-A_e/(A_i - A_e)]V_E \qquad (2)$$

Three ingots designated 5, 10, and X-4, were examined in this study. These were melted at rates of 3.7, 4.3, and 6.4 lb/min. Table 1 gives the process data for the three ingots at a time corresponding to an ingot height of 10 inches (25 cm) from the starting plate. These data include the cross-sectional area of the electrode, voltage, current, slag pool temperature, electrode velocity, slag/metal interface velocity, and the melting rate. All three ingots had cross-sectional areas of 58 square inches.

Table 1. PROCESS VARIABLES AT INGOT MIDHEIGHT

Ingot	A_e ($in.^2$)	Fill Ratio	Volts	Amps	Slag Temp. (°C)	V_E (cm/min)	V_I (cm/min)	M (lb/min)
5	31.92	0.5504	21.5	3420	1627	0.4678	0.5726	3.700
10	31.14	0.5369	25.0	4500	1660	0.5736	0.6651	4.298
X-4	31.14	0.5369	28.0	6800	1782	0.8496	0.9851	6.336

Area of Ingot cross section = 58 sq in.

A_e = area of electrode cross section
V_E = electrode velocity
V_I = slag/metal interface velocity
M = melt rate

The liquid metal pool profiles were determined from ingots 10 and X-4, in which the liquidus isotherms were marked by periodic tungsten additions. These ingots were sectioned longitudinally and one half of each was Blanchard ground and macroetched with a 15% solution of ammonium persulfate. This revealed the ingot macrostructures and the liquidus isotherm shapes as delineated by the marks. Figures 2 and 3 show the macrostructures of these ingots and provide tables of the important process variables corresponding to each of the marks.

Specimens for microstructural analysis were prepared from surface-to-center transverse sections of all three ingots at a height of 10 inches from the starting plate. These were polished and etched with Oberhoffer's reagent to reveal the secondary dendritic structure on the longitudinal face and the primary dendritic structure on the transverse face. Figure 4 shows photomicrographs of the primary and secondary dendritic structures of ingot 5 at the ingot mid-radius. The secondary dendrite arm spacings were measured with an optical microscope at a number of locations between the ingot surface and the centerline. These measurements were fitted with a least-squares regression fit to give the secondary dendrite arm spacing (DAS) in micrometers as a function of the distance from the ingot surface x in centimeters.

$$DAS = a_o + a_1 x + a_2 x^2 \qquad (3)$$

where a_o, a_1, a_2 = regression coefficients.

Mark	Time (min)	Ram (cm)	S/M Height (cm)	Liquidus Height Surface (cm)	Liquidus Height Center (cm)	Pool Depth (cm)	Melt Rate (lb/min)	Pool Velocity (cm/min)
1	27				9.53		3.494	0.540
2	42	9.50	22.18	21.23	15.57	6.61	4.180	0.647
3	52	15.24	29.04	28.10	21.78	7.26	4.298	0.665
4	64	22.20	37.20	36.43	29.88	7.52	4.415	0.683
5	80	31.88	48.27	47.30	40.37	7.90	4.567	0.707

Figure 2. Macrostructure of Ingot 10.

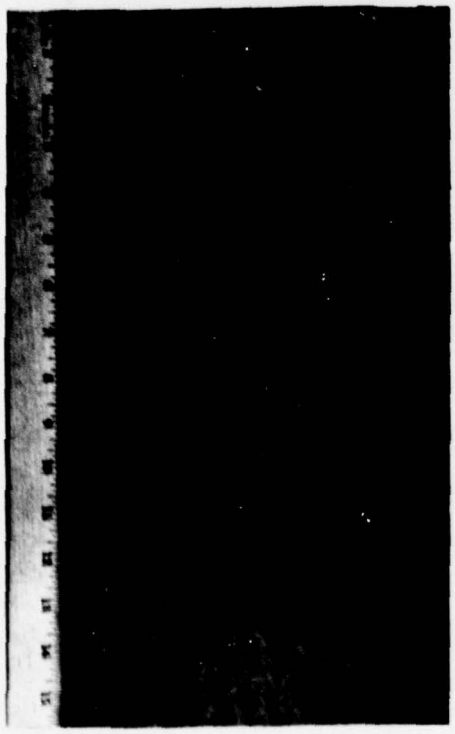

Mark	Time (min)	Ram (cm)	S/M Height (cm)	Liquidus Height Surface (cm)	Liquidus Height Center (cm)	Pool Depth (cm)	Melt Rate (lb/min)	Pool Velocity (cm/min)
3	36	12.60	24.52	22.68	15.32	9.20	6.287	0.973
4	44	19.33	32.44	30.60	21.04	11.40	6.336	0.985
5	51	25.48	39.42	37.68	26.78	12.64	6.471	1.00
6	56	29.64	44.01	42.42	31.10	12.91	6.280	0.972

Figure 3. Macrostructure of Ingot X-4.

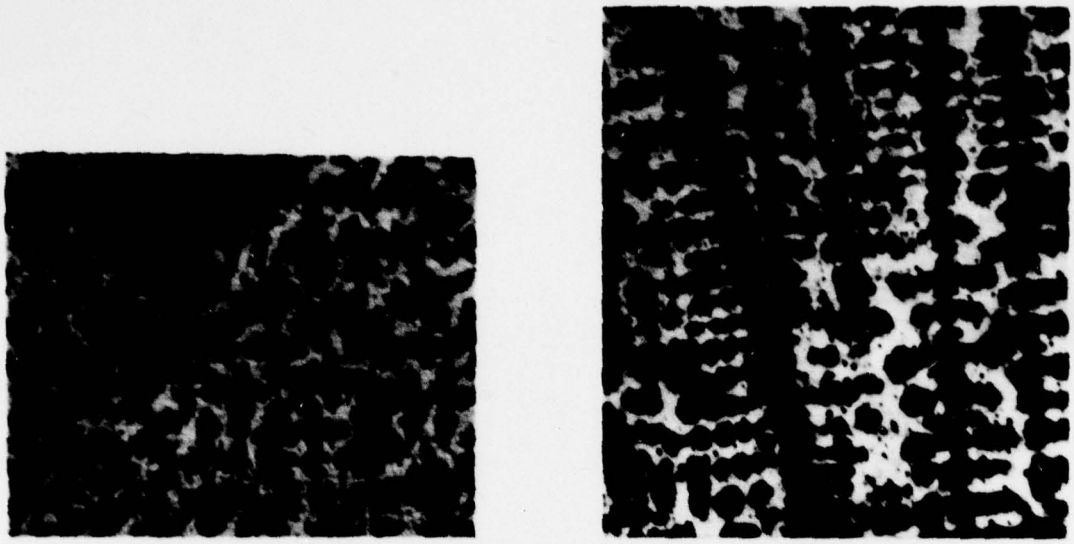

Primary Dendrites
Mag. 10X

Secondary Dendrites
Mag. 15X

Figure 4. Primary and secondary dendritic structures from Ingot 5.

Wet chemical analyses were obtained on both the electrodes and the ingots from drillings at random locations over a transverse section. Table 2 provides the chemistries of the electrodes and the ingots, and the losses resulting from electroslag remelting. Ingots 5 and X-4 were examined for macrosegregation by wet chemical analysis of drillings taken at about 1.5-cm increments from the surface to the center of the ingot at a height of 10 inches from the starting plate.

Table 2. CHEMICAL ANALYSIS OF ELECTRODES AND INGOTS

Ingot		Analysis Weight Percent							
		C	Mn	Si	Ni	Cr	Mo	P	S
5	Electrode	0.39	0.78	0.33	1.76	0.80	0.56	0.008	0.012
	Ingot	0.37	0.73	0.25	1.67	0.77	0.55	0.006	0.002
10	Electrode	0.41	0.77	0.28	1.81	0.82	0.26	0.010	0.009
	Ingot	0.40	0.73	0.19	1.78	0.82	0.27	0.008	0.001
X-4	Electrode	0.41	0.77	0.28	1.81	0.82	0.26	0.010	0.009
	Ingot	-	0.79	0.16	1.75	0.84	0.24	-	-

EXPERIMENTAL RESULTS AND DISCUSSION

Liquidus Isotherm Geometry

The tungsten marks in ingots 10 and X-4 show that the liquidus isotherm profile is hyperbolic in the transverse section. The hyperbolic shape is indicated by the fact that the marked isotherm approaches an asymptote as it nears the ingot surface. Figure 5a is a schematic of the hyperbolic liquidus isotherm shape. The z axis is parallel to the ingot axis, and the x axis is perpendicular to the side

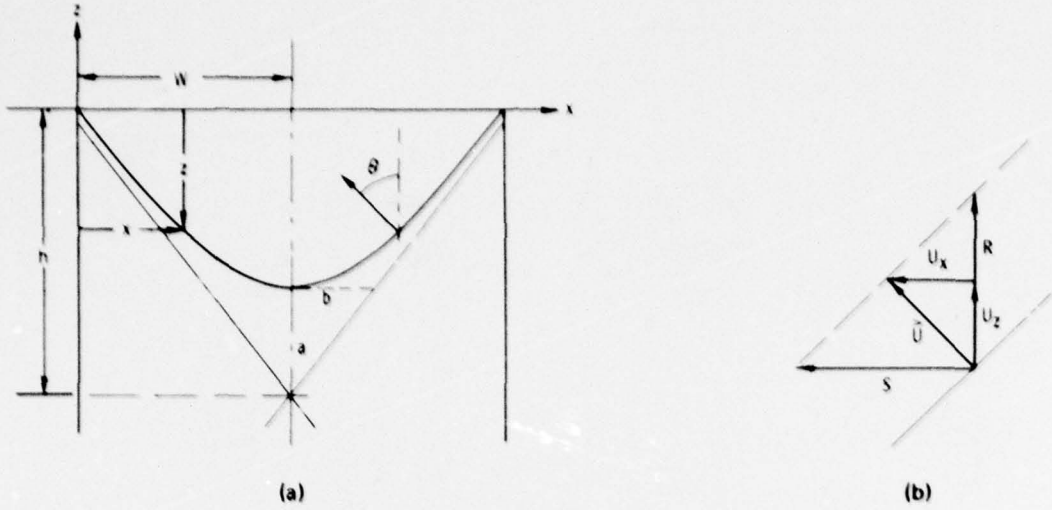

Figure 5. Schematic of hyperbolic liquidus isotherm shape.

of the ingot. The transverse axis is labeled x rather than r because the ingot cross section is round-cornered square rather than circular. The origin of the coordinate system is placed at the intercept of the marked isotherm with the ingot surface; thus, distance along the x axis represents the distance solidified from the mold wall.

The equation representing the hyperbolic liquidus isotherm shape is:

$$\left((z + c)^2/a^2\right) - \left((x - w)^2/b^2\right) = 1 \qquad (4)$$

where c = translation along the z axis from the origin to the center of the hyperbola

w = translation on the x axis from the origin to the axis of the hyperbola (ingot half width)

a,b = constants

Let θ be the angle between the ingot axis and the normal to the liquidus isotherm at any point; then the slope of the isotherm is tan θ. The depth and slope of the isotherm are determined at any distance from the ingot surface as:

$$z = a/b[(x - w)^2 + b^2]^{\frac{1}{2}} - c \qquad (5)$$

$$dz/dx = \tan \theta = a(x - w)/b[(x - w)^2 + b^2]^{\frac{1}{2}} \qquad (6)$$

The constants in the above equations were determined by least-squares regression fits to the isotherm shapes measured from the tungsten marks. Figure 6 shows the regression-fitted liquidus isotherm shapes for ingots 10 and X-4. These show excellent correlation with the pool shapes on the macroetched sections of these

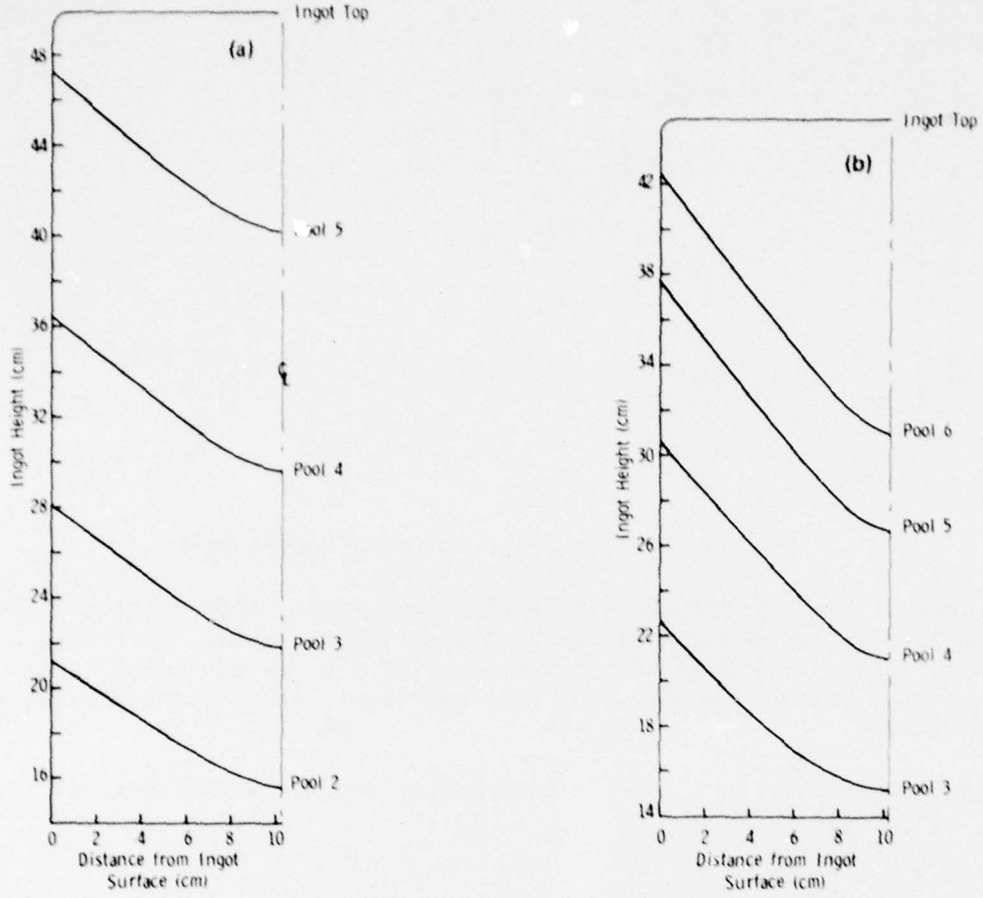

Figure 6. Liquidus isotherm geometries for (a) Ingot 10 and (b) Ingot X-4.

ingots shown in Figures 2 and 3. The multiple correlation coefficients for the regression fits were in excess of 0.999 for all cases. The effect of the bottom chill of the mold on heat transport geometry is shown by the change in shape of the liquidus isotherm with increasing ingot height. The isotherm shape near the bottom of the ingot is shallow and has a large radius of curvature at the ingot centerline, indicating that the bottom chill is increasing the thermal gradient in the axial direction. As ingot height increases, the slope of the isotherm becomes steeper, the radius of curvature at the bottom decreases, and the marked isotherm profiles approach a constant shape indicative of steady state heat transport conditions.

The hyperbola provides an excellent analytical description of the individual liquidus isotherm geometries over a range of melt rates and distances from the bottom of the ingot. However, use of the hyperbolic isotherm shape as a predictive model requires generalization so that the isotherm shape (hyperbolic constants) may be determined as a function of the melting rate or the slag/metal interface velocity.

The effect of the melt rate on solidification geometry can be investigated by examining the transverse solidification rate V_T, which is the rate of growth of the solidified thickness at a constant ingot height. The transverse solidification rate may be determined from the tungsten-marked liquidus isotherm shapes by transforming from x-z coordinates to an x-time coordinate system in which the time t equals the pool depth divided by the slag/metal interface velocity:

$$t = z/V_I \tag{7}$$

Consider a thin horizontal slice of the ingot with a thickness Δz illustrated in Figure 7a. The slice is initially molten, and it progressively solidifies from the mold wall to the ingot centerline as the liquid metal pool and the liquidus and solidus isotherms move past in the axial direction. In x-time coordinates (Figure 7b) solidification progresses in the x direction away from the mold wall as the slice moves forward in time. The x-time coordinate system has been used by Savage and Prichard,[2] Hills,[3] Mizikar,[4] and others for modeling the solidification of continuously cast ingots.

The transformation to x-time coordinates expresses the liquidus shape in terms of the distance of the isotherm from the mold wall as a function of time elapsed since the start of solidification at the mold wall. The expression for the hyperbolic pool shape in x-time coordinates is:

$$[(t + c/V_I)^2/(a/V_I)^2] - [(x - w)^2/b^2] = 1 \tag{8}$$

This relation expresses solidified thickness as a function of time, and it allows a comparison of the solidification of ESR ingots with teemed and continuously cast ingots.

Figure 8 shows comparisons of the experimental liquidus isotherm shapes from the third tungsten mark in ingot 10 and the fourth mark in ingot X-4, both at a height of 25 cm from the starting plate. Figure 8a in x-z coordinates shows a substantial difference in liquidus isotherm shape between the two ingots. Figure 8b shows that the isotherm geometries for the two ingots are almost identical in x-time coordinates, although ingot X-4 was melted at a 47% higher rate than ingot 10. Thus, the transverse solidification velocity and the total time required for solidification to progress from the mold wall to the ingot center appear to be independent of the melt rate.

This empirical relation may be used to predict the shape of the liquidus isotherm in x-z coordinates as a function of the melt rate. The constants for the x-time hyperbolic pool shape (Equation 8) for the third tungsten mark in ingot 10 are:

2. SAVAGE, J., and PRITCHARD, W. H. *The Problem of Rupture of the Billet in the Continuous Casting of Steel.* J. Iron and Steel Inst., v. 178, 1954, p. 269-277.
3. HILLS, A. W. D. *Simplified Theoretical Treatments for the Transfer of Heat in Continuous-Casting Machine Moulds.* J. Iron and Steel Inst., v. 203, 1965, p. 18-26.
4. MIZIKAR, E. A. *Mathematical Heat Transfer Model for Solidification of Continuously Cast Steel Slabs.* Trans. Met. Soc., AIME, v. 239, 1967, p. 1747-1753.

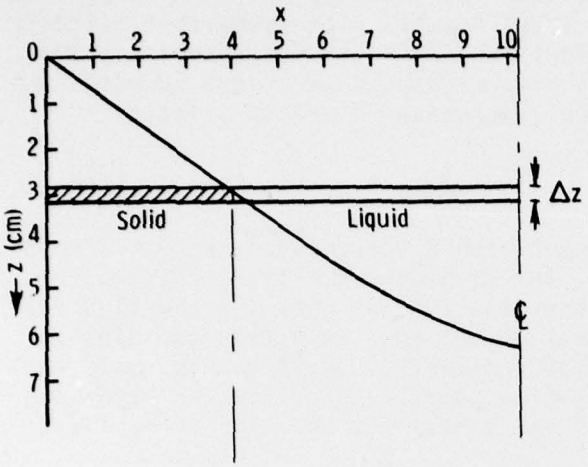

Figure 7a. Illustration of ingot solidification progress.

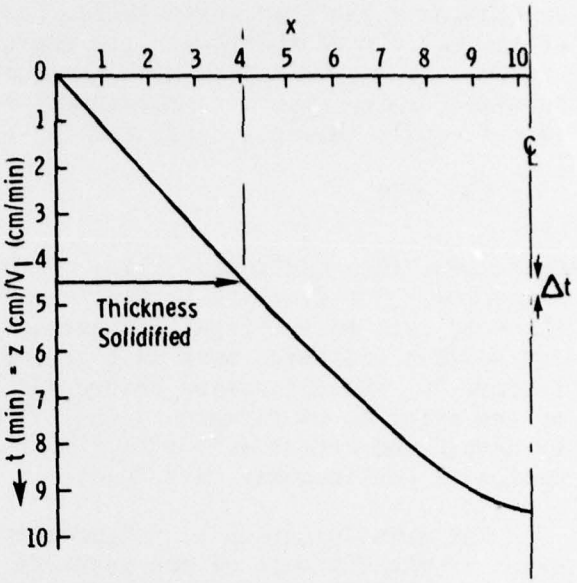

Figure 7b. The x-time coordinate system for modeling the solidification of continuously cast ESR ingots.

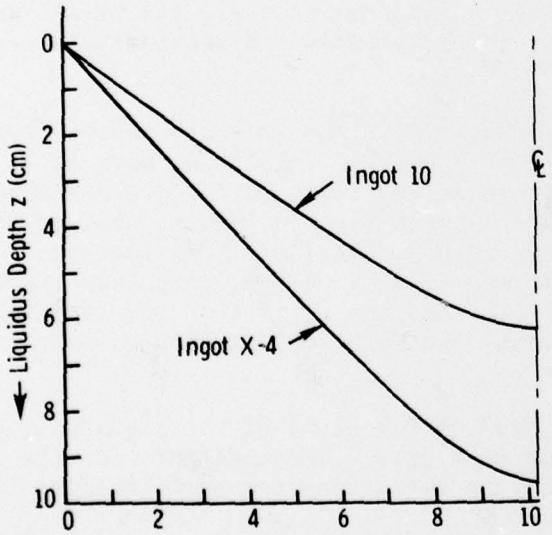

(a) x-z

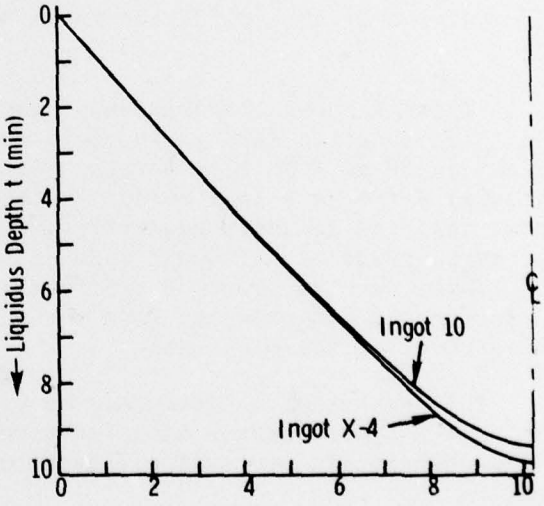

(b) x-time

Figure 8. Liquidus geometry coordinates.

$a/V_I = 2.5306$

$b = 2.2135$

$c/V_I = 7.9269$

The liquidus isotherm geometry in x-z coordinates for any slag/metal interface velocity can be determined by solving for a, b, and c, and substituting these values in Equation 4. Figure 9 shows the predicted isotherm profiles as a function of the melt rate using the above coefficients. The predicted liquidus isotherm shapes are probably valid over a range of melt rates from 3 to 7 pounds per minute. For melt rates less than about 3 lb/min the liquidus isotherm intercepts the slag/metal interface, resulting in a rippled surface and an excessive slag skin thickness. At melt rates in excess of 7 lb/min steam hammering is observed in the crucible.

Local Solidification Time and Mushy Zone Geometry

The previous section developed expressions for the liquidus isotherm geometry as a function of the slag/metal interface velocity. This information can be used, in combination with data on the cooling rate during solidification inferred from dendrite arm spacing measurements, to determine the local solidification time, the depth of the mushy zone, and the location of the solidus isotherm.

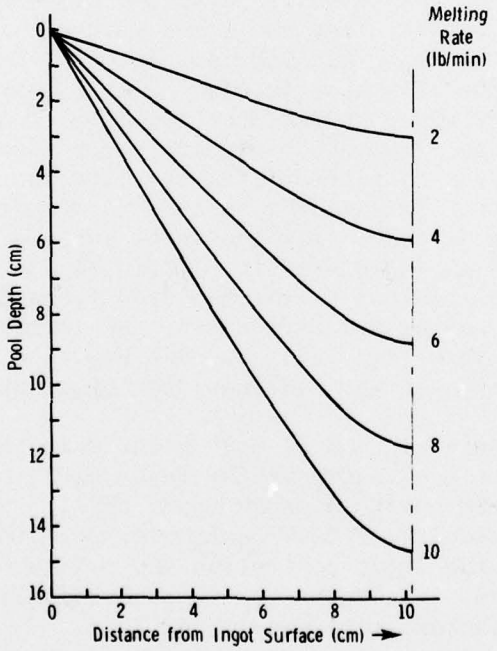

Figure 9. Predicted isotherm profiles as a function of the melt rate.

An empirical power function correlation exists between the average cooling rate during solidification ε and the secondary dendrite arm spacing. This is based on the time available for ripening in which the smaller dendrite arms disappear and the average spacing between arms increases. The correlation was obtained from Mehrabian* for AISI 4340 steel:

$$DAS = 393.66\ \varepsilon^{-0.3082} \tag{9}$$

where DAS = secondary dendrite arm spacing (micrometers)
ε = average cooling rate (°C/min)

The local solidification time t_f is equal to the freezing range for a particular alloy divided by the average cooling rate:

$$t_f = (T^\circ_{liquidus} - T^\circ_{solidus})/\varepsilon \tag{10}$$

The liquidus and solidus temperatures for AISI 4340 steel are given by Basaran et al.[5] as 1483 C and 1427 C; the freezing range is then 56 C. The axial distance between the liquidus and solidus isotherms at a particular distance from the ingot surface is the product of the local solidification time and the slag/metal interface velocity:

$$z_l - z_s = V_I t_f \tag{11}$$

Figure 10 is a plot of the secondary dendrite arm spacings for the three ingots as a function of distance from the ingot surface; the measurements were made at a distance of 25 cm from the starting plate. Near the ingot surface the arm spacings were small for all three ingots (60 to 80 micrometers), but a large difference in arm spacings was observed near the ingot centerline. The centerline dendrite arm spacings ranged from 200 micrometers for ingot 5 to 340 micrometers for ingot X-4. Figure 11 shows plots of the liquidus and solidus isotherm geometries for the three ingots. Data on the mushy zone geometries are given in Table 3 at one-cm increments of distance from the ingot surface. These data include: the depth of the liquidus isotherm from the origin at its intercept with the ingot surface, the slope of the liquidus θ, the measured secondary dendrite arm spacing, the average cooling rate during solidification, the local solidification time, the axial width of the mushy zone ($z_l - z_s$), and the depth of the solidus isotherm calculated from the location of the liquidus and the mushy zone width.

Ingots 5 and 10 (Figure 11a and b) have relatively shallow liquid metal pools with depths equal to about one fourth of the ingot width. Ingot 5 was melted at the lowest rate of 3.7 lb/min with a power input of 21.5 volts and 3400 amps, and a slag/metal interface velocity of 0.57 centimeter per minute. This produced a pool depth of 5.39 cm at the ingot centerline and a liquidus isotherm slope of 32.6° at the ingot surface. The mushy zone width was relatively narrow, and the secondary dendrite arm spacings were small.

*MEHRABIAN, R., University of Illinois, private communication.

5. BASARAN, M., KATTAMIS, T. Z., MEHRABIAN, R., and FLEMINGS, M. C. *A Study of Heat and Fluid Flow in Electroslag Remelting.* Massachusetts Institute of Technology, Contract DAAG46-73-C-0088, Final Report, Army Materials and Mechanics Research Center, AMMRC CTR 74-36, April 1974.

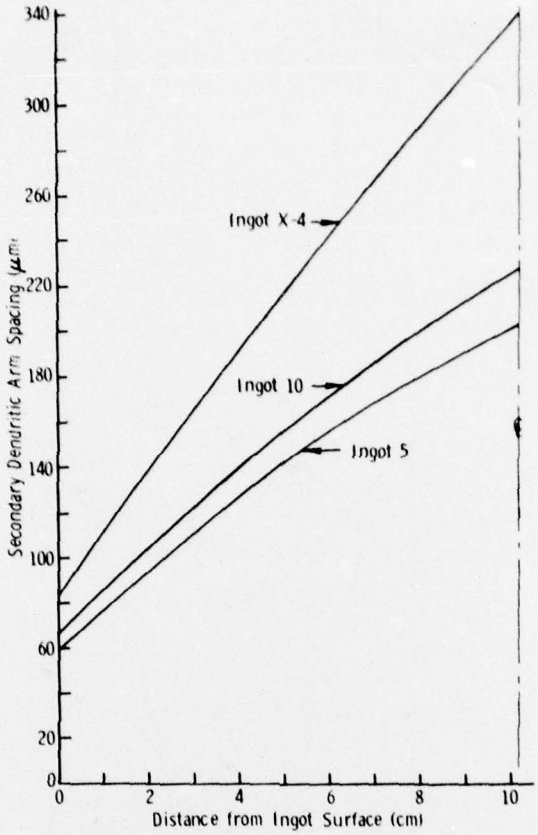

Figure 10. Plot of secondary dendrite arm spacings for three ingots as a function of distance from the ingot surface.

Ingot 10 was melted at a higher power level of 25 volts and 4500 amps, which produced a melt rate of about 4.3 lb/min and a slag/metal interface velocity of 0.67 centimeter per minute. The liquid metal pool had a slightly greater depth of 6.25 cm at the ingot centerline, and the slope of the liquidus isotherm was about 36.6° at the ingot surface. The dendrite arm spacings were larger, and the mushy zone was wider.

Ingot X-4 (Figure 11c) was melted at 28 volts and 6800 amps which produced a very high melt rate for this size crucible of 6.4 lb/min, and a slag/metal interface velocity of about 1 centimeter per minute. The liquid metal pool depth was 9.26 cm at the ingot centerline, the slope of the liquidus was about 47.7° at the ingot surface, the dendritic structure was coarse, and the mushy zone was very wide. The slope of the solidus isotherm near the center of the ingot was about 80°, and the local solidification time at the center was 34 minutes. This coarse structure, wide mushy zone, and long local solidification time provided an excellent opportunity for macrosegregation caused by the flow of interdendritic liquid.

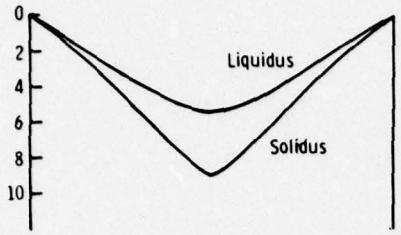

(a) Ingot 5

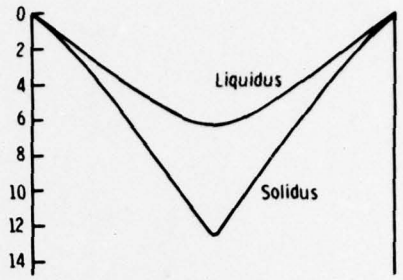

(b) Ingot 10

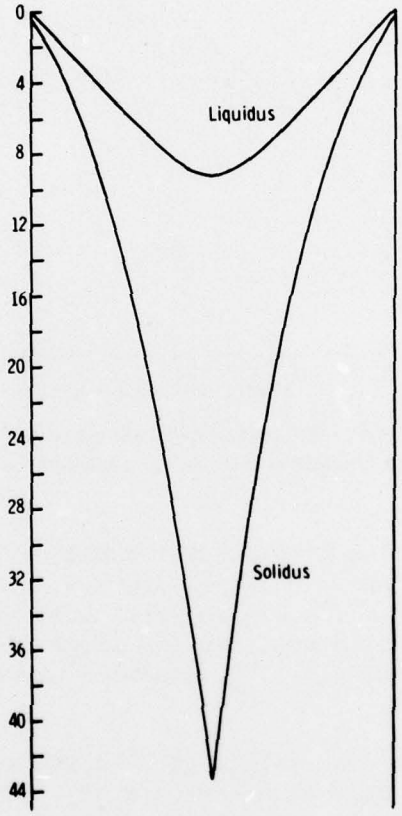

(c) Ingot X-4

Figure 11. **Liquidus and solidus isotherm geometries of three ingots, as they would be obtained under steady state melting conditions. The proximity of the bottom chill in ingot X-4 produced an actual solidus isotherm with less depth than shown and with a lower axial velocity than that of the slag/metal interface.**

Table 3. SOLIDIFICATION DATA FOR INGOT 5

Ingot	X	Z_e	Z_s	$Z_e - Z_s$	θ	DAS	ε	t_f
5	0	0	0.07	0.065	32.61	58.2	494.0	0.113
	1	0.64	0.79	0.150	33.48	75.3	214.2	0.261
	2	1.27	1.56	0.287	32.29	92.0	111.8	0.501
	3	1.90	2.40	0.497	32.04	109.0	64.5	0.868
	4	2.53	3.31	0.783	31.65	125.4	40.9	1.368
	5	3.14	4.29	1.154	31.06	141.3	27.8	2.015
	6	3.73	5.29	1.558	30.08	155.0	20.6	2.721
	7	4.29	6.28	1.985	28.30	167.0	16.2	3.466
	8	4.79	7.24	2.454	24.77	178.3	13.1	4.287
	9	5.19	8.18	2.986	17.32	189.4	10.7	.214
	10	5.38	8.96	3.580	3.37	200.3	9.0	6.235
	10.2	5.39	9.10	3.709	0	202.5	8.6	6.478
10	0	0	0.11	0.111	36.62	65.6	335.7	0.167
	1	0.74	1.00	0.257	36.47	84.9	144.8	0.381
	2	1.46	1.97	0.489	36.28	103.6	76.1	0.736
	3	2.21	3.03	0.820	36.0	121.4	45.4	1.233
	4	2.93	4.19	1.257	35.61	138.5	28.6	1.890
	5	3.64	5.45	1.805	34.98	154.9	20.6	2.713
	6	4.33	6.79	2.462	33.93	170.4	15.1	3.102
	7	4.98	8.21	3.227	32.02	185.2	11.5	4.851
	8	5.56	9.65	4.090	28.19	199.3	9.1	6.149
	9	6.02	11.07	5.042	19.92	212.6	7.4	7.581
	10	6.25	12.32	6.071	3.91	225.1	6.1	9.127
	10.2	6.25	12.54	6.284	0	327.5	5.9	9.448
X-4	0	0	0.34	0.340	47.65	82.1	62.1	0.899
	1	1.09	1.98	0.885	47.60	10.2	62.3	0.899
	2	2.19	4.01	1.824	47.40	137.6	30.3	1.851
	3	3.27	6.52	3.351	47.11	154.5	17.0	3.300
	4	4.43	9.59	6.353	46.69	190.7	10.5	5.333
	5	5.39	13.29	7.904	46.02	316.3	7.0	8.023
	6	6.40	17.67	11.364	44.89	341.2	4.9	11.450
	7	7.37	22.74	15.382	42.81	365.6	3.6	15.614
	8	8.24	28.52	20.296	38.44	289.3	2.7	20.602
	9	8.91	34.95	26.030	28.22	312.3	2.1	26.423
	10	9.25	41.84	32.597	5.79	334.7	11.7	33.085
	10.2	9.26	43.26	34.010	0	339.1	1.6	34.924

X = distance from ingot surface (cm)
Z_e = liquidus depth (cm)
Z_s = solidus depth (cm)
$Z_e - Z_s$ = mushy zone width (cm)
θ = liquidus slope (degree)
DAS = secondary dendrite arm spacing (μ)
ε = average cooling rate (°C/min)
t_f = local solidification time (min)

Figure 12 shows the local solidification times for the three ingots as a function of the distance from the ingot surface. The local solidification time is inversely proportional to the thermal gradient; therefore, solidification takes place rapidly near the ingot surface where the thermal gradients are high, and requires a much longer time near the centerline of the ingot. Ingot X-4 shows a rapid increase in solidification time (decrease in thermal gradient) with increasing distance from the ingot surface. Ingots 5 and 10 which were melted at lower rates show a much smaller change in solidification rate over the ingot cross section.

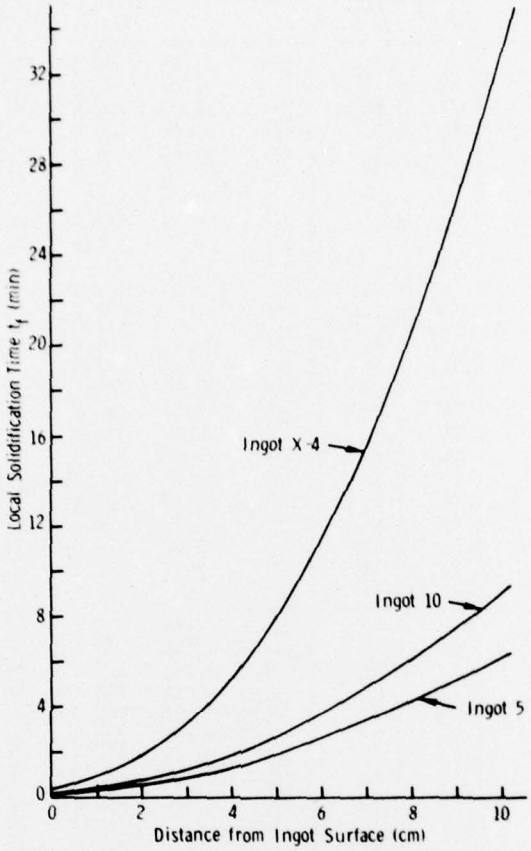

Figure 12. Local solidification times for three ingots as a function of the distance from the ingot surface.

Effect of the Melt Rate on Solidification

For a given alloy and ingot size the melt rate or slag/metal interface velocity is the most important variable affecting the solidification structure and geometry; the melt rate is also the principal variable used for process control. An examination of the experimentally marked liquidus isotherm shapes in the preceding two sections led to an empirical model of the liquidus shape as a function of the melt rate. This model indicates that the transverse solidification velocity is melt-rate independent, and that the shape of the liquidus in x-z coordinates is, therefore, a linear function of the melt rate. This linear variation of the liquidus geometry with the melt rate was illustrated in Figure 9.

An examination of the solidus isotherm geometries in Figure 11 indicates that the depth of the solidus and the width of the mushy zone are not related to the melt rate in the same linear fashion. The depth of the solidus increases rapidly with increasing melt rate. At high melt rates such as that used for ingot X-4 this produces a wide centerline mushy zone typical of continuously cast ingots.

The effect of the melt rate on the liquidus and solidus isotherm shapes is illustrated in Figure 13, which shows the centerline isotherm depths as functions of the slag/metal interface velocity. The centerline depth of the liquidus varies in a linear manner as predicted. The centerline depth of the solidus isotherm, however, increases approximately with the cube of the slag/metal interface velocity.

Melt control of many commercial ESR furnaces is based on the relation between the melt rate and the liquid metal pool depth; the slope of the liquidus isotherm, which can be easily located by marking, determines the columnar dendrite orientation and hence the orientation of the macrostructure. The more important solidification variables, however, are more strongly reflected by the location of the solidus isotherm than by the liquidus. These include the thermal gradients, local solidification time, mushy zone width, and the potential for macrosegregation. Since these variables do not scale linearly with the melt rate, empirical rules have been developed which relate the melt rate and liquid pool depth to the onset of solidification-related defects.

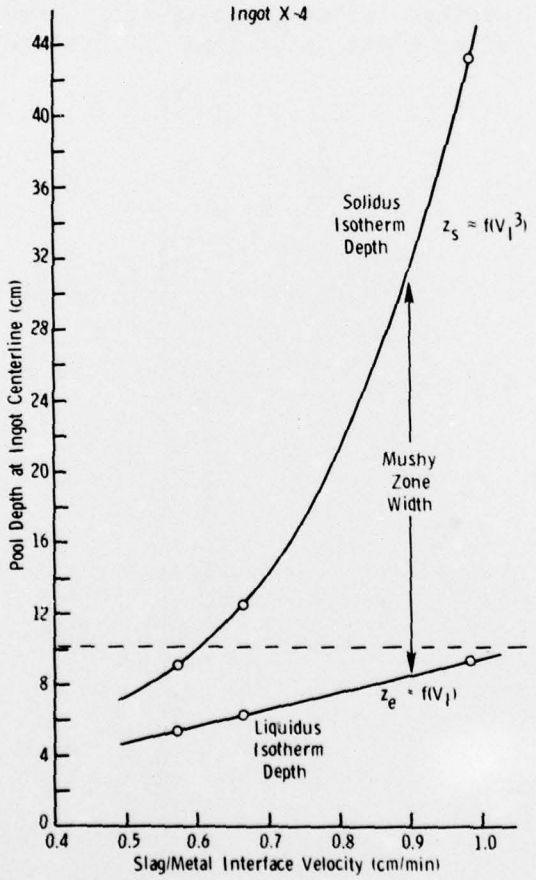

Figure 13. Effect of melt rate on the liquidus and solidus isotherm shapes.

Comparisons of liquid pool geometry are usually based on the slope of the liquidus isotherm or on the ratio of the liquid pool depth to the ingot radius. A high melt rate is desirable for reasons of melting efficiency (kilowatt-hour/ton) and furnace productivity; however, an upper limit is imposed by the increased probability for solidification defects. The upper limit for satisfactory melting is generally considered to be that rate at which the pool depth equals the ingot radius, or where the slope of the liquidus isotherm reaches 45 degrees. Examination of Figure 13 illustrates the validity of this rule. For ingot X-4 the liquid metal pool depth is approximately equal to the ingot half width, and the depth of the solidus isotherm and width of the mushy zone are both increasing very rapidly with increasing slag/metal interface velocity. Figures 14 and 15 show the axial mushy zone width and the local solidification time at the ingot center plotted as functions of the liquidus isotherm slope at the ingot surface. Both are increasing rapidly at a liquidus slope of 45 degrees.

Figures 16, 17, and 18 illustrate the melt rate dependence of solidification variables as a function of distance from the ingot surface. Figure 16 shows the secondary dendrite arm spacings versus the slag/metal interface velocity at the ingot surface, at the quarter width (5 cm from the surface), and at the ingot

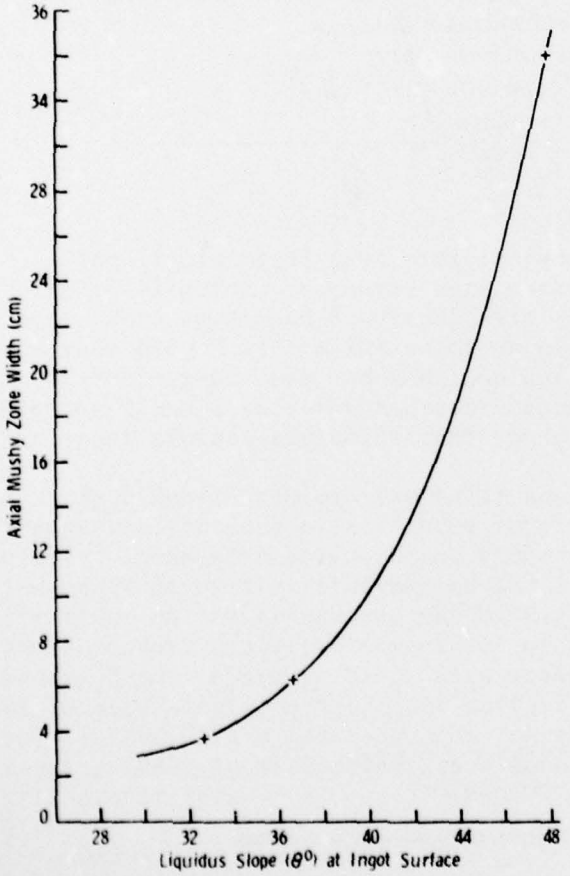

Figure 14. Axial mushy zone width as a function of the liquidus isotherm slope at ingot surface.

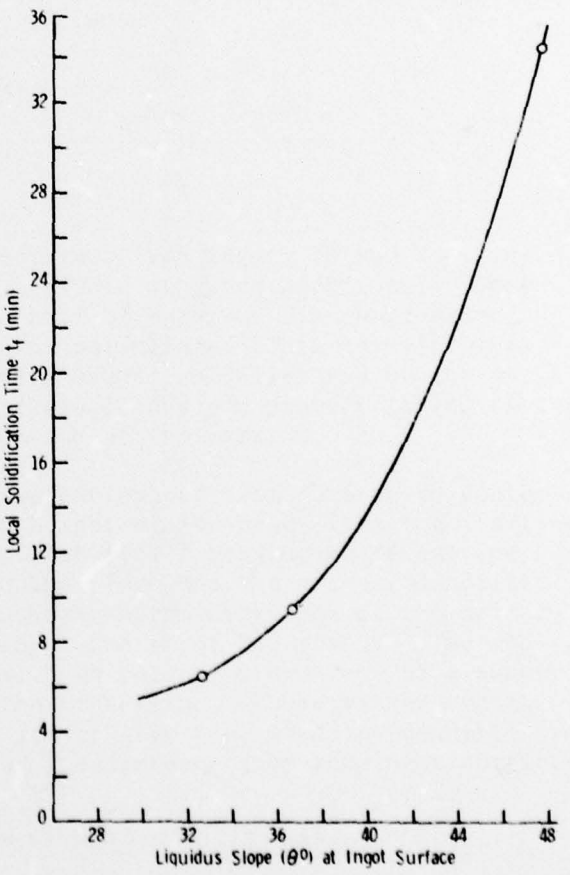

Figure 15. Local solidification time as a function of the liquidus isotherm slope at ingot surface.

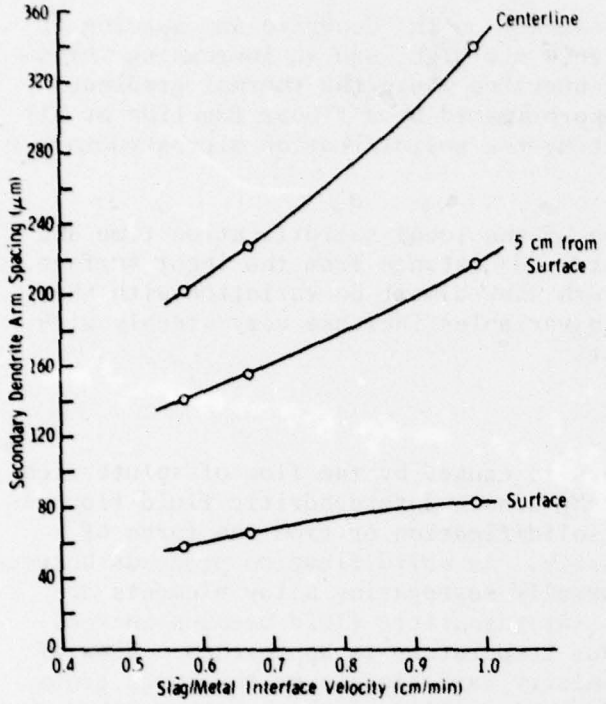

Figure 16. Effect of slag/metal interface velocity on the secondary dendrite arm spacing.

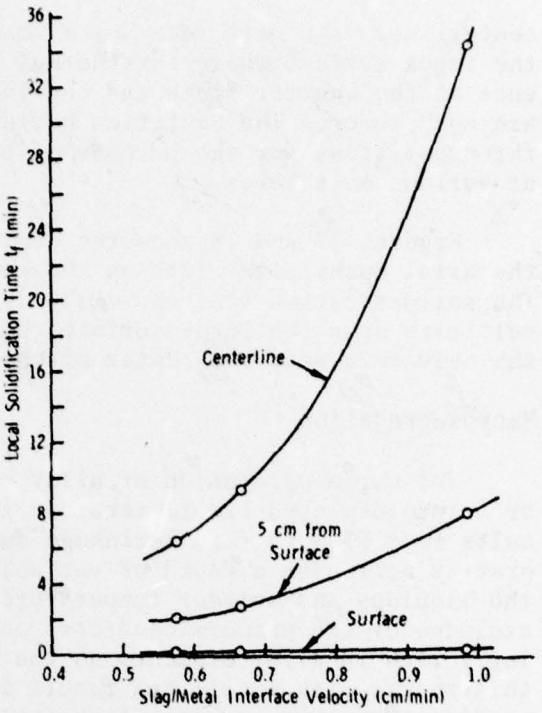

Figure 17. Effect of slag/metal interface velocity on the local solidification time.

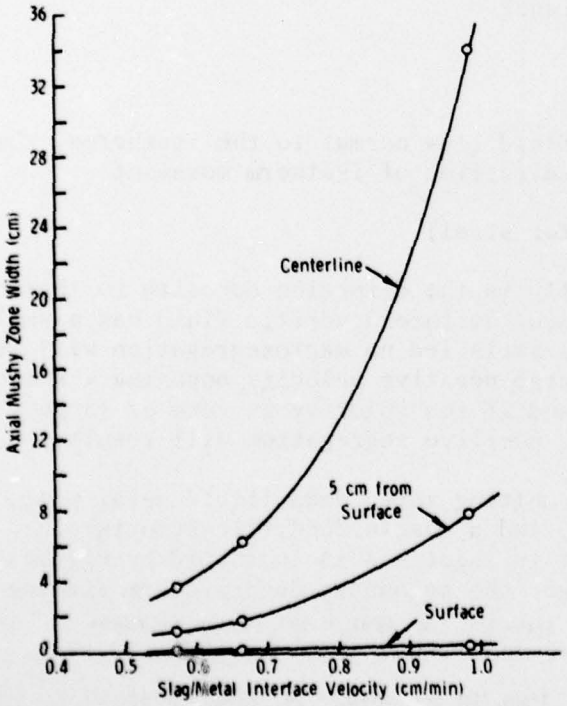

Figure 18. Effect of slag/metal interface velocity on the axial width of the mushy zone.

centerline. The melt rate has a small influence on the dendrite arm spacing at the ingot surface where the thermal gradients are high, and an increasing influence at the quarter width and the ingot centerline where the thermal gradients are much lower. The variation could be approximated by a linear function at all three positions for the purpose of predicting the solidification microstructure at various melt rates.

Figures 17 and 18 show the dependence of the local solidification time and the axial mushy zone width on the melt rate and distance from the ingot surface. The solidification time and mushy zone width show almost no variation with the melt rate near the ingot surface, but both variables increase very steeply with the melt rate near the center of the ingot.

Macrosegregation

The macrosegregation of alloy elements is caused by the flow of solute-rich or solute-depleted liquid metal in the mushy zone. Interdendritic fluid flow results from flow to feed shrinkage during solidification or from the force of gravity acting on a fluid of variable density. As solidification proceeds between the liquidus and solidus temperatures, normally segregating alloy elements are excluded by the primary dendrites and the interdendritic fluid becomes increasingly rich in alloy elements as the solidus temperature is approached. Flow of this solute-rich liquid can result in chemistry variations over the ingot cross section or in the erosion of channels and the formation of channel segregates.

The relations between the velocity of the interdendritic fluid flow, the isotherm velocities, and macrosegregation have been quantified by Flemings, Mehrabian, and Nereo,[6-8] and are summarized by Mehrabian:[9]

$$V_n/\overline{U} = -\Omega/1 - \Omega$$

where V_n = velocity of the interdendritic fluid flow normal to the isotherms, the positive direction being in the direction of isotherm movement
$\overline{U}$ = isotherm velocity
Ω = solidification shrinkage (0.03 for steel)

The interdendritic flow velocity is generally in the direction opposite to that of the isotherms, that is, it is negative. When the interdendritic fluid has a small negative velocity and the above equation is satisfied no macrosegregation will result. If the interdendritic fluid has a large negative velocity opposing the isotherms, negative segregation will result; and if the velocity is zero or is positive in the direction of isotherm movement, positive segregation will result.

Macrosegregation is favored by a high melting rate, deep liquid metal pool, large mushy zone, long solidification time, and a coarse dendritic structure. These conditions are expected to be present in ingot X-4 as indicated by Figures 11, 12, and 13. Near the center of the ingot the secondary dendrite arm spacing

6. FLEMINGS, M. C., and NEREO, G. E. *Macrosegregation: Part I.* Trans. Met. Soc., AIME, v. 239, 1967, p. 1449-1461.
7. FLEMINGS, M. C., MEHRABIAN, R., and NEREO, G. E. *Macrosegregation, Part II.* Trans. Met. Soc., AIME, v. 242, 1968, p. 41-49.
8. FLEMINGS, M. C., and NEREO, G. E. *Macrosegregation, Part III.* Trans. Met. Soc., AIME, v. 242, 1968, p. 50-55.
9. MEHRABIAN, R. *Segregation Control in Ingot Solidification* in Solidification Technology, 1974, p. 299-315, Proc. Army Conf. on Solidification Technology.

was 339 micrometers, the axial width of the mushy zone was 34 cm, and the local solidification time was 34 minutes. Ingot 5 was melted at the lowest rate, and it should therefore be the least likely of the three ingots to exhibit macrosegregation. Near the centerline of ingot 5 the dendrite arm spacing was 200 micrometers, the axial mushy zone width was only 3.7 cm, and the local solidification time was only 6.5 minutes.

Figure 19 shows the chemical composition of ingots 5 and X-4 as a function of distance from the ingot surface. These results are based on the wet chemical analysis of drilled chips taken at approximately 1.5-cm increments from the ingot surface to the center. The analyses show no apparent macrosegregation present in any of the alloy elements, at either the low melt rate used for ingot 5 or at the very high melt rate used for ingot X-4. The conclusion must be that density-driven macrosegregation in AISI 4340 steel is not produced by the thermal and geometric conditions of solidification present in these experiments.

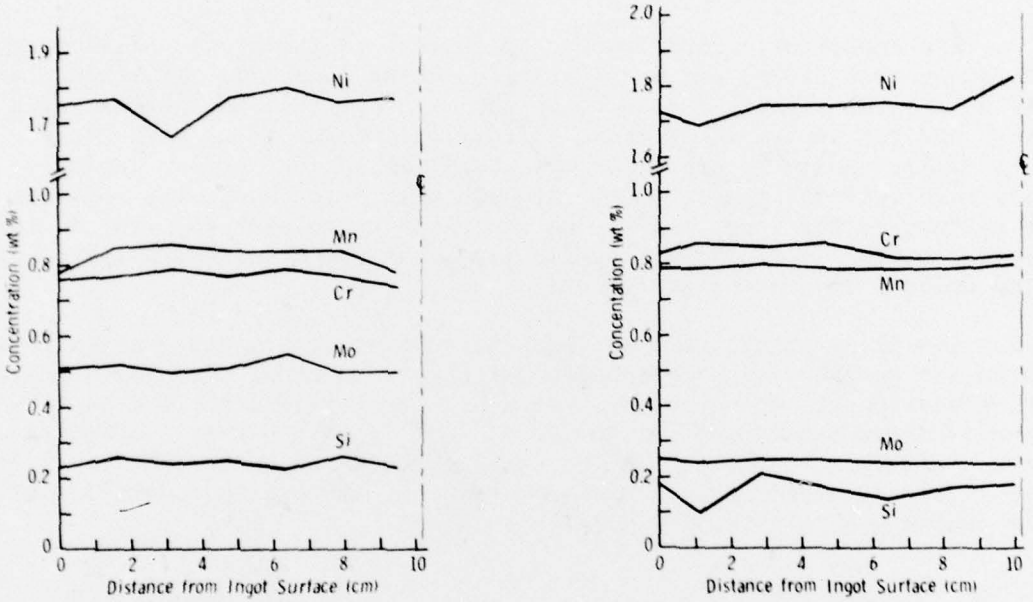

Figure 19. Chemical analysis.

CONCLUSIONS

1. For the round-cornered square mold used in these experiments the liquidus isotherm shape is hyperbolic in the longitudinal section perpendicular to the ingot face. This indicates an almost constant rate of growth of the solidified thickness for the first few centimeters from the mold wall. The hyperbolic liquidus isotherm geometry may be typical for slab molds in the direction perpendicular to the face of the slab.

2. At a sufficient ingot height that the liquid metal pool has assumed a steady shape, the liquidus isotherm profile may be predicted as a function of the slag/metal interface velocity by means of an empirical model. This model is based on the premise that the transverse solidification velocity and the time required to solidify the ingot cross section are independent of the slag/metal interface velocity. The hyperbolic liquidus isotherm shape is, therefore, a linear function of the interface velocity.

3. The average cooling rate during solidification and the local solidification time may be determined from measurements of the secondary dendrite arm spacing and an empirical relationship between the arm spacings and the cooling rate for a particular alloy. This information in combination with knowledge of the liquidus isotherm geometry and the slag/metal interface velocity can be used to determine the axial width of the mushy zone and the location of the solidus isotherm.

4. The important solidification variables, including the solidus isotherm depth, mushy zone width, and local solidification time, are not linear functions of the melt rate. Within 3 to 4 cm of the ingot surface the thermal gradients are high and the variation of these solidification variables with increasing melt rate is small. Near the center of the ingot the solidification variables increase rapidly with increasing melt rate. At high melt rates where the liquidus isotherm depth approaches the ingot radius and its slope approaches 45°, the solidus depth, mushy zone width, local solidification time, and potential for solidification-related defects increase significantly.

5. Low alloy steels such as the AISI 4300 series do not seem susceptible to macrosegregation caused by density variations in the interdendritic fluid. No macrosegregation was detected, even at a high melt rate where the depth of the solidus isotherm reached 43 cm, the local solidification time reached 34 minutes, and the solidification structure was coarse. This indicates that low alloy steels can be safely remelted at much higher rates than segregation-sensitive alloys with larger contents of high or low density solutes.